Ceramics International 44 (2018) 18727–18735

Contents lists available at ScienceDirect

Ceramics International

journal homepage: www.elsevier.com/locate/ceramint

Perovskite oxide-based nanohybrid for low-temperature thin-film solid oxide fuel cells fabricated *via* a facile and scalable electrochemical process

Beom-Kyeong Park[a,b,1,2], Han Gil Seo[b,1], WooChul Jung[b,*], Jong-Won Lee[c,*]

[a] New and Renewable Energy Research Division, Korea Institute of Energy Research, 152 Gajeong-ro, Yuseong-gu, Daejeon 34129, Republic of Korea
[b] Department of Materials Science and Engineering, Korea Advanced Institute of Science and Technology, 291 Daehak-ro, Yuseong-gu, Daejeon 34141, Republic of Korea
[c] Department of Materials Science and Engineering, Chosun University, 309 Pilmun-daero, Dong-gu, Gwangju 61452, Republic of Korea

ARTICLE INFO

Keywords:
Hybrid
Perovskite oxide
Nanoarchitecture
Electrodeposition
Solid oxide fuel cell

ABSTRACT

High-performance electrodes for energy conversion systems can be achieved through the selection of materials with appropriate functionality as well as fabricating the desired nanoarchitectures. Nanohybrids of metal and perovskite metal oxide have a great potential as electrodes owing to the combined advantages of the active constituents; however, the controlled hybridization in nanoscale is hindered by the conflicting nature of the metal and perovskite oxide, and it should involve cost-, energy- and time-intensive fabrication techniques. Here, we report an electrochemical process as a facile, cost-effective, and scalable route to fabricating metal–perovskite metal oxide nanohybrids with tailored architectures. We successfully fabricate a Pt@$LaCoO_3$ nanohybrid that consists of a conformal $LaCoO_3$ nanonetwork on a nanoporous Pt thin-film framework. We examine this nanohybrid as an electrode for thin-film-based, low-temperature solid oxide fuel cells and demonstrate that the synergistic nanostructuring of Pt@$LaCoO_3$ leads to exceptionally high oxygen reduction activity at reduced operating temperature and high stability.

1. Introduction

Along with the rapid development of electrochemical energy conversion and storage devices, such as fuel cells, batteries, and supercapacitors, the demand for high-performance electrodes that can facilitate mass/charge transfer and electrochemical reactions has been increasing sharply [1–4]. Recently, metal–metal oxide nanohybrids have attracted great attention as a promising electrode owing to the following potential advantages [5–12]. First, it is possible to implement all the inherent characteristics of the individual active constituents that make up the hybrid. For example, high electrical conductivity and catalytic properties of the metal can be combined with decent ionic conductivity and structural/chemical stability of the oxide [5,8,10]. Second, it is possible to control the structural factors more freely and broadly to achieve the desired performance. For instance, nanoarchitectures can be designed and fabricated to have (*i*) porous channels for easy access of reactants, (*ii*) short pathways for mass/charge transport, and (*iii*) large specific surface/interface areas for electrochemical redox reactions [3,5,7,11–13]. Among various metal oxides, perovskite-type metal oxides with the chemical formula of ABO_3 (A: rare earth metal, B: transition metal) are considered to be promising constituents of the hybrid electrode [14–16]. In particular, their electrical and electrochemical redox properties can be easily tailored for specific applications by controlling the type and composition of A and B as well as the oxygen nonstoichiometry [14,16,17].

Given the attractive features of hybridization, it is not surprising that metal–perovskite oxide hybrid electrodes can find applications in a variety of electrochemical devices. It has, however, turned out to be difficult to construct a nanoarchitecture suitable for the hybrid system because two materials with different physicochemical properties must be handled together [5,7,18]. In particular, considering the conflicting properties of metals (*e.g.*, low thermal stability and large thermal expansion coefficients) and perovskite oxides (*e.g.*, high-temperature calcination and sintering), heat treatment always presents a big challenge in the entire manufacturing process [19,20]. Moreover, the microstructural and compositional control of multi-component oxides such as perovskites may increase the complexity of the hybrid fabrication. Therefore, the controlled hybridization in nanoscale (*e.g.*, the partial or total modification of a metal surface with a functional perovskite oxide) can only be realized using cost-, energy-, and/or time-

* Corresponding authors.
E-mail addresses: wcjung@kaist.ac.kr (W. Jung), jongwon@chosun.ac.kr (J.-W. Lee).
[1] These authors contributed equally to this work.
[2] Present address. Department of Materials Science and Engineering, Northwestern University, 2220 Campus Dr., Evanston, IL 60208, USA.

https://doi.org/10.1016/j.ceramint.2018.07.102
Received 21 June 2018; Received in revised form 10 July 2018; Accepted 11 July 2018
Available online 14 July 2018

intensive techniques; for example, (*i*) pulsed laser deposition, atomic layer deposition, and magnetron sputtering based on complicated/expensive precursors and equipment or (*ii*) wet chemical infiltration requiring repeated infiltration–drying–annealing treatments [21–23].

The electrochemical processing can be used to deposit a wide range of metals and metal oxides including perovskite and fluorite-type oxides, and it has been recently reported that the conformal oxide coatings with controlled nanostructures can be formed on the conductive and/or non-conductive substrates with complex shapes *via* electrochemical processes [24–27]. Here, we report a facile, cost-effective, and scalable way to fabricate nanohybrids of metal and perovskite oxide *via* electrochemical processing. As a case study, a perovskite oxide ($LaCoO_3$; designated as LCO) nanonetwork was conformally formed on a nanoporous metal (Pt) thin-film framework (Pt@LCO nanohybrid) through an electrochemical process, namely, chemically assisted electrodeposition (CAED). The CAED process was conducted at ambient temperatures and pressures, had a fast deposition rate, and required only minimal energy input. Moreover, it was carried out using an aqueous solution with relatively simple precursors and placed no limit on the shape and area over which the material was deposited. The feasibility of this nanohybrid was investigated as a cathode (oxygen electrode) for low-temperature solid oxide fuel cells (LT-SOFCs). In this study, an LCO perovskite with catalytic and mixed ionic-electronic conducting properties was chosen as the active constituent of the hybrid to investigate the beneficial role of hybridization in enhancing the oxygen reduction kinetics on the Pt metal (a benchmark electrode material for thin-film-based LT-SOFCs) [28–30]. As will be shown later, the synergistic Pt@LCO interactions led to outstanding electrochemical performance and durability under LT-SOFC operating conditions.

2. Experimental

2.1. Fabrication of metal-perovskite metal oxide nanohybrids

A (100) single-crystal yttria-stabilized zirconia (YSZ, $(Y_2O_3)_{0.08}(ZrO_2)_{0.92}$, MTI Corp.) (thickness ~ 0.5 mm) was used as an O^{2-}-conducting electrolyte (substrate) and prepared as a square-shaped coupon with dimensions of 10 mm × 10 mm. A nanoporous Pt thin-film was used as a metal framework and was obtained by thermal decomposition of a sputter-deposited PtO_x film. A dense PtO_x film of ~ 100 nm thickness was deposited on the YSZ substrate using oxygen reactive DC magnetron sputtering equipped with a three-inch Pt target. The sputtering was carried out at a DC power of 50 W and a constant working pressure of 10 mTorr in a gas mixture of Ar and O_2 (Ar: O_2 = 1:1 in volume). Then, a nanoporous Pt thin-film framework was obtained by subsequent heat-treatment of an as-deposited PtO_x film in air at 600 °C for 1 h. An electrochemical cell consisting of cathodic and anodic chambers was prepared for electrodeposition. The cathodic chamber contained an YSZ substrate coated with a Pt thin-film framework (working electrode), an Ag/AgCl reference electrode (with saturated NaCl), and a mixed nitrate solution of $La(NO_3)_3{\cdot}6H_2O$ (99.99%, Kanto) and $Co(NO_3)_2{\cdot}6H_2O$ (≥ 99.0%, Aldrich). The concentrations of La^{3+} and Co^{2+} in the metal nitrate solution were 16 mM and 14 mM, respectively, and the solution pH was adjusted to 2.7 by adding 0.1 M HCl. The anodic chamber contained a Pt mesh (counter electrode) and a 30 mM KNO_3 solution (≥ 99.0%, Aldrich). The two chambers were separated by an anion-exchange membrane (APS4, Asahi Glass). Electrodeposition was galvanostatically conducted at room temperature by the application of a cathodic current density of 0.6 or 3 mA cm^{-2}. After rinsing with distilled water and drying at 70 °C, the specimens were heat-treated in air at 550 °C for 1 h.

2.2. Material characterizations

The phases and crystal structures of the nanohybrids were identified by X-ray diffraction (XRD, 2500 D/MAX, Rigaku) with Cu K_α (λ = 1.5405 Å) radiation. The morphologies and microstructures were observed by scanning electron microscopy (SEM, Hitachi SU–8230) and transmission electron microscopy (TEM, FEI Tecnai G^2 F30 S-Twin). The surface chemistry was investigated by X-ray photoelectron spectroscopy (XPS, Thermo MultiLab 2000 spectrometer) combined with energy dispersive X-ray spectroscopy (EDS, Ametek). An inductively coupled plasma mass spectroscopy (ICP–MS, Agilent) was employed to determine the chemical composition.

2.3. Electrochemical experiments

A symmetric cell structure with identically sized (10 mm × 10 mm) Pt@LCO electrodes on both sides of the YSZ electrolyte was used to evaluate the electrochemical performance of the nanohybrid as a cathode for thin-film-based LT-SOFCs. The AC-impedance spectra of the cells were measured at temperatures of 300–500 °C and at oxygen partial pressures of 0.05–1.00 atm. The impedance measurement was carried out at an open-circuit voltage (OCV) using a Bio-Logic VSP–300. An AC amplitude of 20 mV at a frequency range of 4 MHz–2 MHz was used. The perturbation voltage of 20 mV was chosen in this work so that it would lie within the linear regime of the sample's current–voltage response. In addition, an accelerated stability test was performed in a temperature range of 500–700 °C for 100 h.

3. Results and discussion

Fig. 1(a) illustrates a schematic diagram of the fabrication process of a Pt@LCO nanohybrid electrode on an YSZ electrolyte along with SEM images taken at each step. A nanoporous Pt thin-film was used as a metal framework and was obtained by thermal decomposition of a sputter-deposited PtO_x film [11,30]. Because the PtO_x thin film formed by oxygen reactive sputtering was not thermodynamically stable, the short heat-treatment produced numerous nanoscale pores by rapidly releasing the oxygen present inside the film. The resulting film exhibited percolating Pt networks with interconnected nanopores, which served as an efficient oxygen gas pathway. A conformal $LaCoOH_x$ nanonetwork was synthesized on the nanoporous Pt thin-film framework through the CAED process, and then, it was "*in-situ*" converted to perovskite-type LCO during SOFC start-up.

The CAED involved the electrochemical reduction of nitrate species (NO_3^-), followed by the chemical precipitation of $LaCoOH_x$, as schematically illustrated in Fig. 1(b). Upon application of a cathodic overpotential, the reduction of NO_3^- at the working electrode (Pt framework) resulted in an increase in the concentration of OH^-, thereby increasing the local pH near the electrode surface [31,32]. The increased pH subsequently induced metal ions (La^{3+} and Co^{2+}) to be chemically co-precipitated as $LaCoOH_x$. Fig. 1(c) exhibits the variation of the cathodic potential with time monitored during the CAED process. When the CAED was carried out at a cathodic current density of 0.6 mA cm^{-2}, the potential decreased rapidly with time and reached a steady-state value as low as − 0.68 V *vs.* Ag/AgCl. The measured potential was much lower than the equilibrium redox potential of NO_3^- (− 0.19 V *vs.* Ag/AgCl), and thus, the electric charge would be mostly consumed by the NO_3^- reduction rather than by the reduction of La^{3+} and Co^{2+} into their metallic states [31]. Given the redox potential of Co^{2+} (− 0.48 V *vs.* Ag/AgCl), we cannot rule out the possibility of Co electrodeposition, in which Co^{2+} is directly reduced to an insoluble metallic form [31]. However, no metallic Co species was detected in the XRD pattern of the as-deposited film (Fig. S1). As shown in Fig. 1(c), the Pt thin-film framework became olive-colored after CAED for 6 min, indicating the formation of $LaCoOH_x$ on its surface. Thereafter, $LaCoOH_x$ was converted to perovskite-type LCO upon mild heat-treatment for material characterizations. It should be pointed out that, in practice, the thermal conversion of hydroxide to oxide would be achieved "*in-situ*" during an initial heating step (SOFC start-up) at the operating

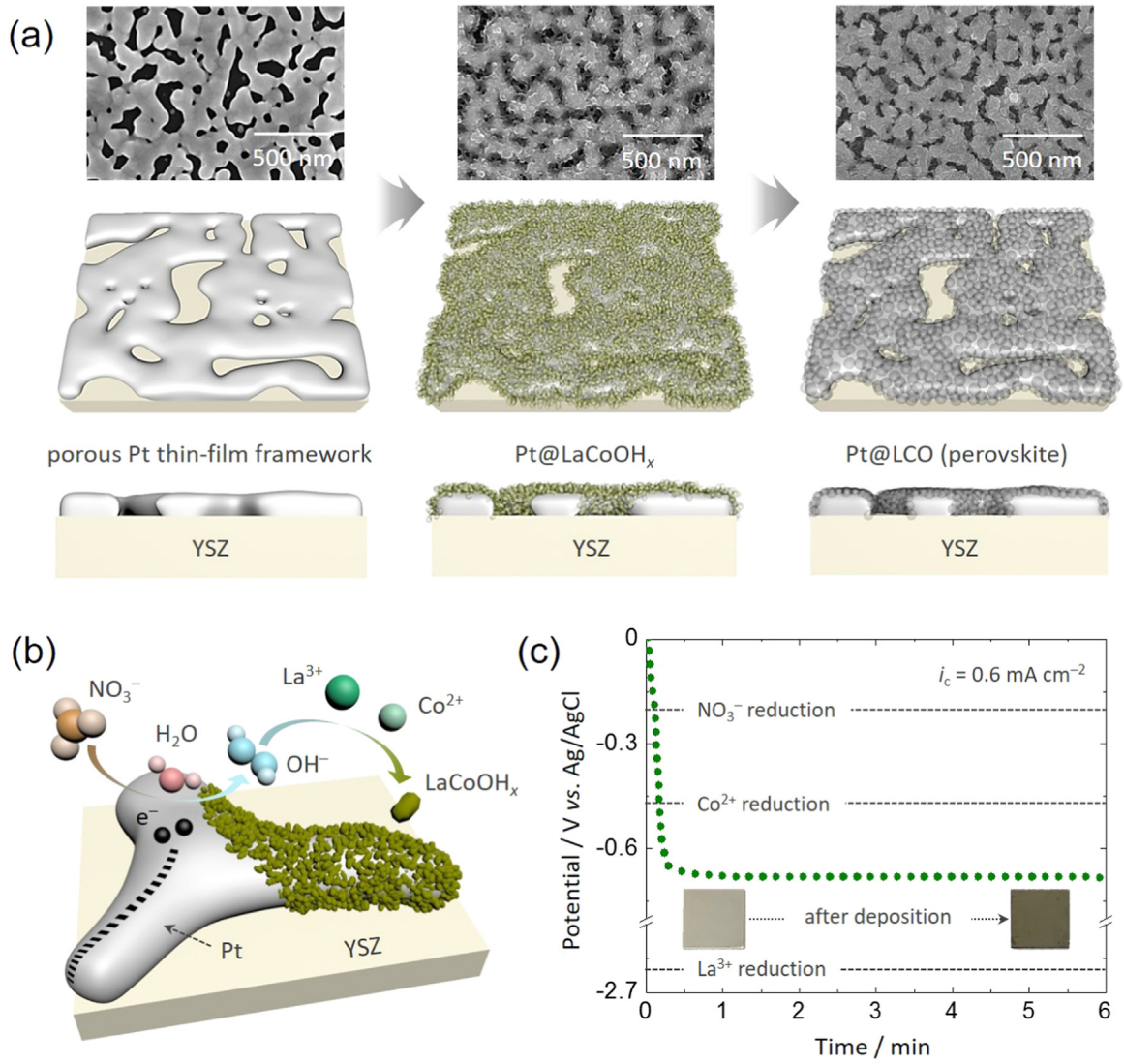

Fig. 1. (a) Schematic diagram of the fabrication process of a Pt@LCO nanohybrid electrode on an YSZ electrolyte along with the SEM micrographs. (b) Synthesis mechanism of $LaCoOH_x$ on the Pt thin-film framework *via* CAED. (c) Potential *vs.* time profile measured during the CAED process of $LaCoOH_x$ at a cathodic current density of 0.6 mA cm^{-2} and photographs of the pristine and $LaCoOH_x$-coated Pt frameworks.

temperature without the need for additional heat-treatment process.

For practical applications to LT-SOFC cathodes, the hybrid architecture should be engineered to have a conformal perovskite oxide network (on the metal framework), which is thin enough to allow facile ionic conduction as well as to induce strong synergistic interactions between the perovskite and the underlying metal [5,7]. Keeping this design requirement in mind, a parametric study of the CAED process was conducted to tailor and optimize the architecture of the Pt@LCO nanohybrid. As shown in Fig. 2, the morphological feature of LCO was examined as a function of the applied current density (i_c) and the deposition time (t) (see Fig. S2 for low-magnification SEM micrographs). The CAED process with i_c = 0.6 mA cm^{-2} and t = 6 min led to the formation of a uniquely architectured hybrid (designated as Pt@LCO(1)), in which a percolated LCO nanonetwork made of tiny particles was conformally deposited on the nanoporous Pt thin-film framework. In comparison to Pt@LCO(1) synthesized at i_c = 0.6 mA cm^{-2}, Pt@LCO(2) prepared at i_c = 3 mA cm^{-2} had discrete LCO agglomerates. When the CAED was carried out for a longer deposition time (t = 30 min), on the other hand, a Pt thin-film framework was completely covered by thick and heavily cracked LCO coatings (Pt@LCO(3) and Pt@LCO(4)), so that its original nanoporous structure was no longer preserved (see Fig. S3 for the cross-sectional SEM image of the Pt framework). In this case, the electrochemical properties of Pt@LCO(3) and Pt@LCO(4) would be exclusively determined by LCO rather than by the synergistic interaction of Pt and LCO. The results indicated that a conformal $LaCoOH_x$ nanonetwork was formed *via* the slow precipitation reaction induced by a low current density of 0.6 mA cm^{-2} (Pt@LCO(1)), and then, it grew but cracked (Pt@LCO(3)) due to heavy precipitates with further progressing CAED. Meanwhile, during the CAED with i_c = 3 mA cm^{-2}, the high cathodic polarization (about − 1.3 V *vs.* Ag/AgCl) caused water electrolysis accompanied by hydrogen evolution. Thus, conformal but discrete agglomerates formed in the early stage (Pt@LCO(2)), and some part of the deposit was delaminated by sever hydrogen evolution in the later stage (Pt@LCO(4)). Based on the above experiments on the morphological control, Pt@LCO nanohybrids with conformal LCO networks (Pt@LCO(1)) and discrete LCO agglomerates (Pt@LCO(2)) were subjected to comprehensive physicochemical and electrochemical characterizations.

Prior to detailed electrochemical study of the synthesized nanohybrids, the physical and chemical properties of Pt@LCO were characterized using various analytical tools. The XRD patterns of the Pt@LCO(1) nanohybrid on YSZ showed the characteristic peaks corresponding to perovskite-type LCO (JCPDS No. 48-0123), and the crystallite size of LCO was estimated to be ~ 12 nm from the half-width of

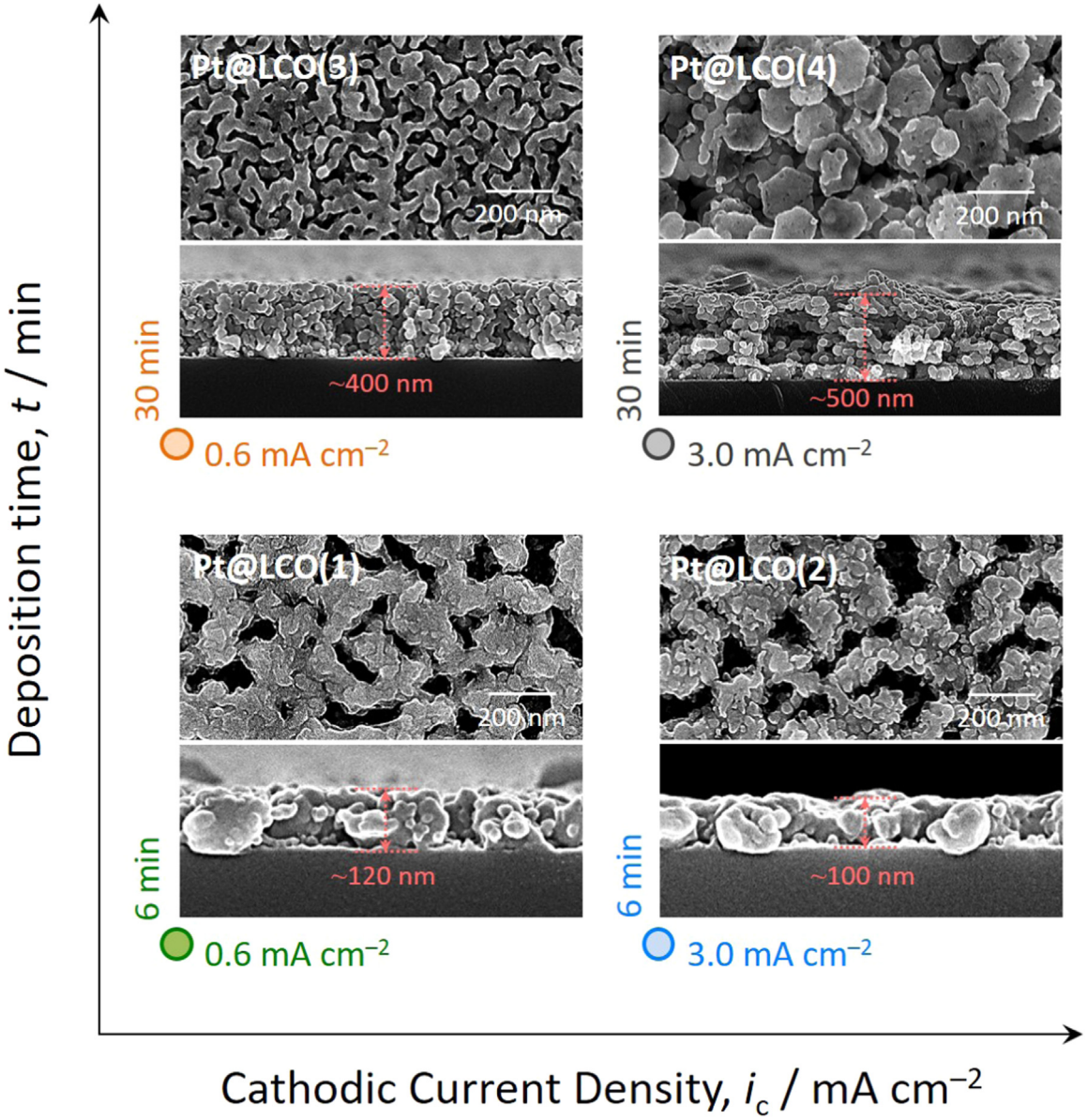

Fig. 2. Surface and cross-sectional SEM micrographs of the Pt@LCO nanohybrid electrodes synthesized *via* the CAED processes with various parameters: Pt@LCO(1), i_c = 0.6 mA cm^{-2} and t = 6 min; Pt@LCO(2), i_c = 3.0 mA cm^{-2} and t = 6 min; Pt@LCO(3), i_c = 0.6 mA cm^{-2} and t = 30 min; Pt@LCO(4), i_c = 3.0 mA cm^{-2} and t = 30 min.

the (110) peak (Fig. S1). The surface chemistry of Pt@LCO(1) was characterized by XPS and EDS analyses (Fig. 3). The O 1s XPS spectrum exhibits two peaks at the binding energy (BE) values of 528.6 eV and 530.3 eV, which are ascribed to the lattice oxygen species (O^{2-}) and the adsorbed oxygen species (O_2^{2-} or O^-), respectively. The XPS spectrum for Co 2p is characterized by the two main signals for Co $2p_{3/2}$ and Co $2p_{1/2}$ at BE = 778.9 eV and 793.9 eV, respectively, along with satellite peaks. The La 3d XPS spectrum has two spin-orbit components of La $3d_{5/2}$ and La $3d_{3/2}$, each of which exhibits a double-peak structure (BE = 833.7 eV and 837.1 eV for La$3d_{5/2}$ and BE = 850.2 eV and 853.7 eV for La $3d_{3/2}$) associated with electron transfer from oxygen ligands to La 4f. The chemical composition of LCO was determined as $LaCo_{0.94}O_{3-\delta}$ by ICP–MS. The slight Co deficiency (Co/La ratio ~ 0.94) was reconfirmed by XPS (Fig. 3). The Co deficiency in LCO is known to produce oxygen vacancies for charge compensation, which in turn leads to improved oxygen ionic conductivity and surface activity for oxygen reduction [33,34].

The Pt@LCO(1) nanohybrid was examined by TEM to acquire detailed information on the nanostructured interfaces among Pt, LCO, and YSZ (Fig. 4). The cross-sectional TEM and elemental distribution analyses (Fig. 4(a)) revealed that an LCO nanonetwork (thickness ~ 20 nm) was conformally formed on the Pt framework (thickness ~ 50 nm and width ~ 150 nm), and it was composed of nanoparticles (size ~ 10–20 nm) and nanopores between them. The high-resolution TEM micrographs (Fig. 4(b)) of the interfacial regions, Pt | LCO (region A) and Pt | LCO | YSZ (region B), showed the lattice fringes of d = 0.275 nm and 0.216 nm corresponding to the (110) and (006) crystal planes of the $LaCoO_3$ perovskite, respectively. More importantly, LCO nanoparticles were in intimate contact with Pt and YSZ, forming very cohesive interfaces. In addition, the SEM micrographs (Fig. S4) taken on different regions of the electrode confirmed the formation of uniform LCO nanonetworks over the whole electrode surface, suggesting that the CAED process is easily scalable to the large-area devices.

As an exemplary application, a Pt@LCO nanohybrid was employed as a cathode for thin-film-based LT-SOFCs. For a wide range of technical applications (particularly, portable power generation), thin-film SOFCs

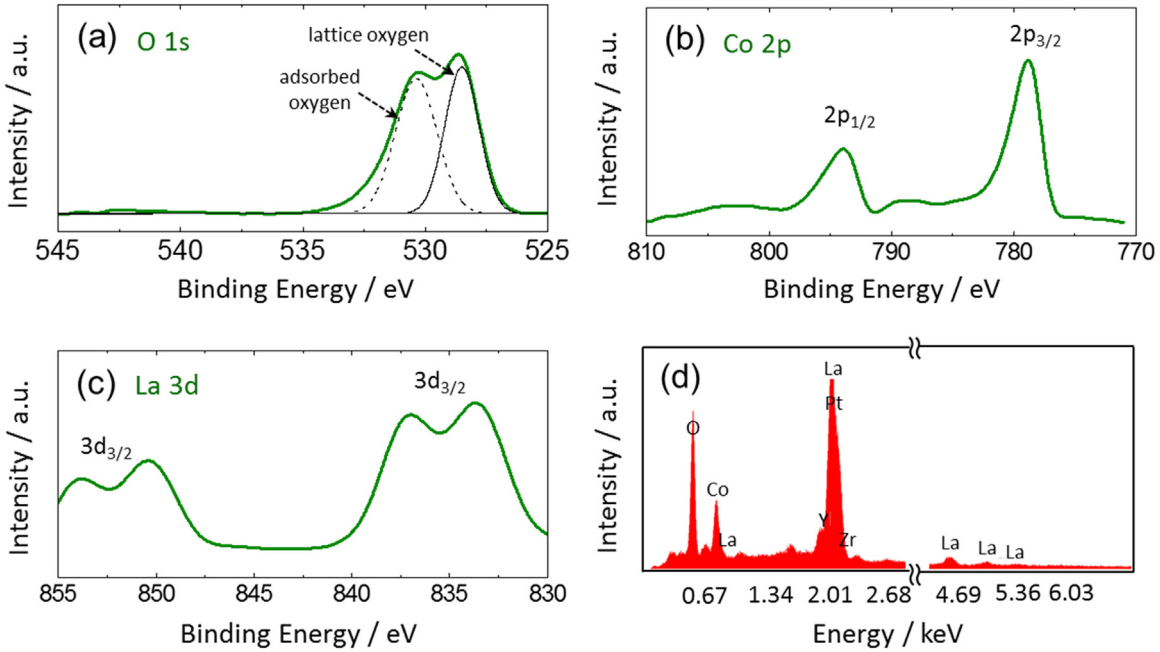

Fig. 3. XPS spectra of the (a) O 1s, (b) Co 2p, and (c) La 3d regions and (d) EDS spectrum obtained for Pt@LCO(1).

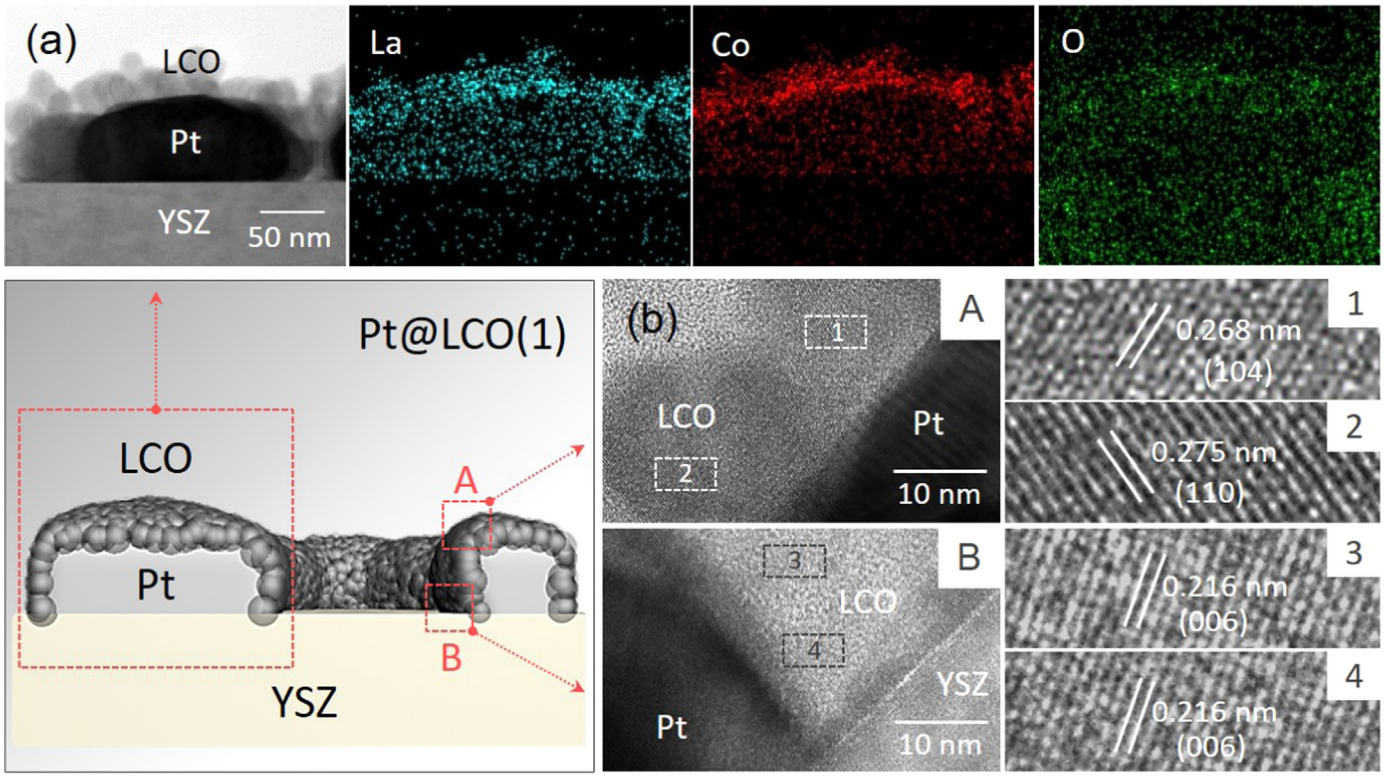

Fig. 4. (a) Cross-sectional TEM micrograph and elemental distribution maps of La, Co, and O for Pt@LCO(1). (b) High-resolution TEM micrographs of the interfacial regions: Pt | LCO (region A) and Pt | LCO | YSZ (region B).

have much promise as efficient devices that can directly convert the chemical energy of fuels into electricity at low temperatures (< 500 °C) [30,35–37]. The thin-film membrane, downscaled to several hundreds of nanometers, allows the lower operating temperatures by reducing the ohmic resistance of a solid electrolyte. In contrast to conventional SOFCs running at elevated temperatures (> 750 °C), thin-film SOFCs have the merits of rapid start-up and shut-down cycles and reduced system cost [35,36]. In addition to the requirement for thin-film electrolytes, however, the poor low-temperature performance of the cathodes associated with the sluggish oxygen reduction reaction (ORR) is a critical "bottle neck" for the realization of thin-film-based LT-SOFCs [35–38]. The Pt@LCO nanohybrid was tested as an LT-SOFC cathode using a symmetric cell with the configuration of Pt@LCO | YSZ | Pt@LCO.

Fig. 5 compares the electrochemical performance of the Pt-only and Pt@LCO nanohybrid electrodes at various operating temperatures (*T*)

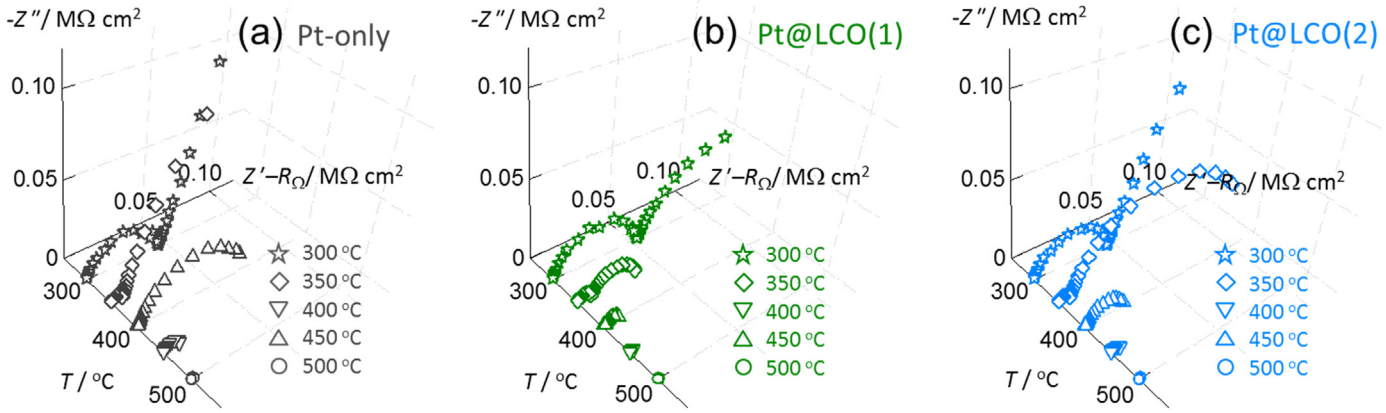

Fig. 5. AC-impedance spectra (Nyquist plots) of the symmetric cells with the (a) Pt-only, (b) Pt@LCO(1), and (c) Pt@LCO(2) electrodes measured at various temperatures and p_{O_2} = 0.21 atm.

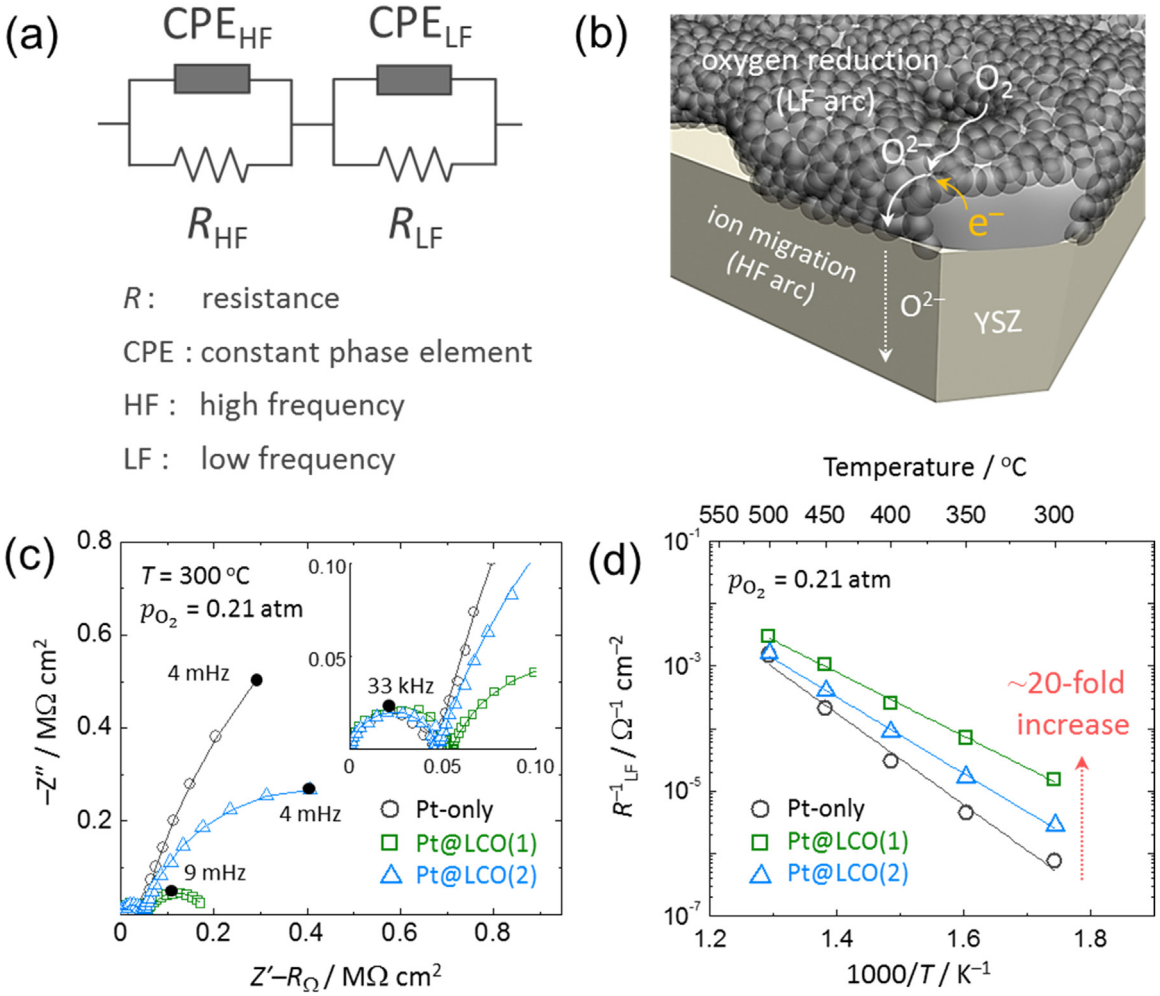

Fig. 6. (a) Equivalent circuit used for fitting of the measured impedance data. The HF and LF arcs are attributed to the O^{2-} migration in the YSZ electrolyte and the ORR at the electrode as schematically shown in (b). Comparison of (c) the AC-impedance spectra of the cells with different electrodes measured at T = 300 °C and p_{O_2} = 0.21 atm and (d) the temperature dependences of the electrode conductance (R_{LF}^{-1}). The solid lines in the Nyquist plots represent the results fitted using the equivalent circuit in (a).

of 300–500 °C. The AC-impedance data in Fig. 5 were measured on the symmetric cells in air (oxygen partial pressure, p_{O_2} = 0.21 atm) at an open circuit voltage (OCV). The real impedance (Z') and imaginary impedance (Z'') values were normalized by the geometric surface area of the electrode. The measured Z' value was subtracted by the uncompensated ohmic resistance (R_Ω) to restrict our discussion to the interfacial reactions. The impedance spectra of the cells with the Pt-only and Pt@LCO hybrid electrodes show two adjacent arcs, which are distinguished as a nearly ideal high-frequency (HF) arc and a slightly distorted low-frequency (LF) arc, respectively. These spectra were modelled by a series of two parallel R–CPE sub-circuits, as shown in Fig. 6(a), where R and CPE represent the resistor and constant phase

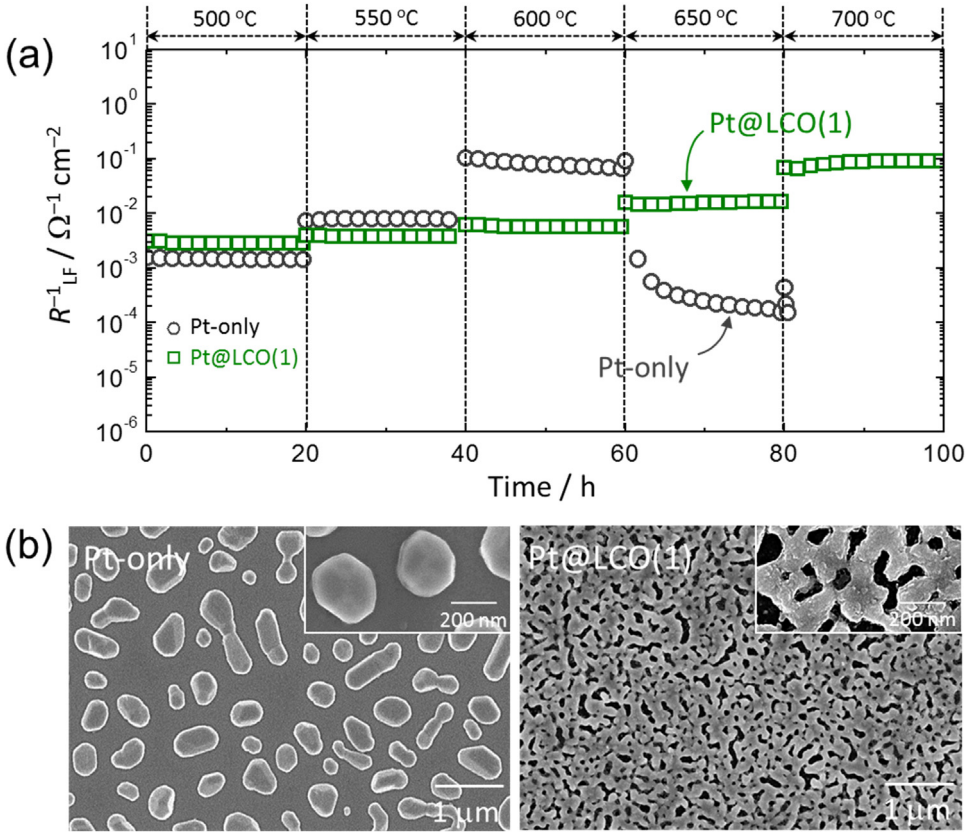

Fig. 7. (a) Evolution of the electrode conductance (R_{LF}^{-1}) of Pt and Pt@LCO(1) estimated from the AC-impedance measurements during the accelerated stability tests at various temperatures and p_{O_2} = 0.21 atm. No reliable impedance measurements from Pt were possible after 81 h, indicating the failure of the Pt-only electrode. (b) Surface SEM micrographs of the Pt-only and Pt@LCO(1) electrodes after continuous testing of 100 h.

element, respectively. The HF arc is attributed to the O^{2-} conduction (migration) in the YSZ electrolyte (Fig. 6(b)) based on the following experimental findings: (*i*) the activation energy (E_a) values derived from R_{HF} were ~ 1.1 eV, regardless of the electrode used (Fig. S5(a)), which is in good agreement with the literature data for YSZ [11], (*ii*) the conductance (R_{HF}^{-1}) was independent of p_{O_2} (Fig. S5(b)), and (*iii*) the HF arc remained unchanged regardless of the LCO coating layer.

Accordingly, the low-frequency (LF) arc is thought to be associated with the electrode polarization, *i.e.*, the ORR at the electrode (Fig. 6(b)). Of particular note is a remarkable reduction in R_{LF} for the Pt@LCO nanohybrid electrodes in comparison with the Pt-only electrode (Fig. 6(c) and S5(c)), which implies the synergetic reaction between Pt and LCO. The Arrhenius plots for the electrode conductance (R_{LF}^{-1}) in Fig. 6(d) show the R_{LF}^{-1} values of 7.4×10^{-7}–1.5×10^{-3} Ω^{-1} cm^{-2} for the Pt-only electrode at 300–500 °C, which are comparable to those reported in the literature on Pt electrodes for thin-film based LT-SOFCs [28,29]. The R_{LF}^{-1} value of Pt@LCO(1) was about 20 times higher than that of Pt at 300 °C. Moreover, the E_a value for the ORR decreased in the order of Pt (~ 1.45 eV) > Pt@LCO(2) (with discrete LCO agglomerate) (~ 1.21 eV) > Pt@LCO(1) (with percolated LCO nanonetwork) (~ 1.01 eV). The R_{LF}^{-1} values seem to be low for practical applications; however, the following points should be considered. First, under bias conditions during fuel cell operations, the R_{LF}^{-1} value for Pt electrode is greatly increased to about 5–10 times [39–41]. Second, the cell performance for LT-SOFCs highly depends on the entire cell configuration, the structures/compositions of the cell components, and the fabrication conditions [42–45]. Through an optimized study, for example, Su et al. reported that an LT–SOFC with a Pt cathode (thickness = 120 nm) exhibits a maximum power density of 677 mW cm^{-2} at 400 °C [45]. Further work is in progress to fabricate LT-SOFCs with Pt@LCO and characterize their electrochemical performance.

Even though a detailed ORR mechanism is beyond the scope of this study, the LCO nanonetwork formed *via* the CAED process modified the Pt electrode in such a way that it effectively enhanced the ORR kinetics at low temperatures. In the Pt-only electrode on the YSZ electrolyte, electrochemically active sites for ORR are restricted to triple-phase boundaries (TPBs) among Pt, YSZ, and gas (pore). LCO has the outstanding ability to absorb, dissociate, and exchange oxygen on its surface, and it can also provide a percolated pathway for ionic conduction from its surface to YSZ. At the same time, the slight Co deficiency in LCO could generate the surface oxygen vacancy, thereby enhancing the ORR kinetics [33,34]. Furthermore, nanopores in the LCO network (see Fig. 4) may serve as a channel for oxygen gas diffusion to the reaction sites. As a result, the catalytically active, mixed ionic-electronic conducting LCO nanonetwork can extend the electrochemical active region from the "one-dimensional" TPBs (Pt | YSZ | gas) to the entire "two-dimensional" surface of the nanohybrid electrode (LCO | gas, LCO | Pt | gas, and LCO | YSZ | gas), which leads to the considerable improvement in electrochemical performance.

One of the most serious concerns of metal-based electrodes for LT-SOFCs is the metal coarsening and agglomerations during continuous operation, which results in loss of TPBs and performance degradation [9,11,46,47]. To investigate this issue, the Pt-only and Pt@LCO(1) electrodes were subjected to "accelerated" stability tests in a temperature range of 500–700 °C, and the evolution of the electrode conductance (R_{LF}^{-1}) was *in-situ* monitored for 100 h (Fig. 7(a)). The operating temperature was increased by 50 °C, and the cells were held at each temperature for 20 h. Although the Pt-only electrode showed higher conductance compared with Pt@LCO(1) at elevated temperatures (> 550 °C), it exhibited serious performance degradation as evidenced by a rapid decrease of the conductance during the stability test. In fact, no reliable measurements on Pt were possible after 81 h,

indicating the failure of the Pt-only electrode. On the other hand, the electrode conductance of Pt@LCO(1) remained almost constant without any signs of failure under harsh operating conditions. The surface morphologies of the tested electrodes were examined using SEM, and the results are shown in Fig. 7(b). It is clearly seen that the nanoporous Pt thin-film framework was transformed to large, spherical, isolated particles (*i.e.*, coarsening and agglomeration), which is believed to be responsible for the observed performance degradation (loss of TPBs). It should be pointed out that the Pt@LCO(1) electrode showed no structural change even after the stability test at 700 °C. These results indicate that the conformal LCO nanonetwork in the Pt@LCO nanohybrid electrode effectively inhibits the atomic diffusion of Pt and thus plays a crucial role in improving the structural stability at elevated temperatures.

4. Conclusions

In this study, we developed a facile, cost-effective, and scalable approach to fabricating metal–perovskite metal oxide nanohybrids with tailored architectures *via* electrochemical processing. We demonstrated the fabrication of a Pt@LCO nanohybrid composed of a conformal LCO nanonetwork on a nanoporous Pt thin-film framework through the CAED process. The CAED approach proposed in this study offers considerable advantages over conventional techniques used for nanoscale hybridization: the CAED is performed in low-cost aqueous solutions using simple equipment, and as in the case of any electrochemical routes, it is easily scalable to large-area devices. When employed as a thin-film-based LT-SOFC cathode, the Pt@LCO nanohybrid electrode exhibited exceptionally high oxygen reduction activity (~ 20-fold improvement as compared with the Pt-only electrode) at a temperature as low as 300 °C and high stability at elevated temperatures, proving that the CAED process may be a feasible approach to developing high-performance hybrid electrodes.

Acknowledgements

This work was supported by the Korea Institute of Energy Technology Evaluation and Planning (KETEP) and the Ministry of Trade, Industry & Energy (MOTIE) of the Republic of Korea (No. 20163030031850). This work was also supported by the Korea Electric Power Corporation (KEPCO) Research Institute.

Appendix A. Supporting information

Supplementary data associated with this article can be found in the online version at doi:10.1016/j.ceramint.2018.07.102.

References

[1] Z. Shao, S.M. Haile, A high-performance cathode for the next generation of solid-oxide fuel cells, Nature 431 (2004) 170–173.
[2] Y.-G. Guo, J.-S. Hu, L.-J. Wan, Nanostructured materials for electrochemical energy conversion and storage devices, Adv. Mater. 20 (2008) 2878–2887.
[3] G. Yu, X. Xie, L. Pan, Z. Bao, Y. Cui, Hybrid nanostructured materials for high-performance electrochemical capacitors, Nano Energy 2 (2013) 213–234.
[4] Z. Gao, L.V. Mogni, E.C. Miller, J.G. Railsback, S.A. Barnett, A perspective on low-temperature solid oxide fuel cells, Energy Environ. Sci. 9 (2016) 1602–1644.
[5] J. Jiang, Y. Li, J. Liu, X. Huang, C. Yuan, X.W. Lou, Recent advances in metal oxide-based electrode architecture design for electrochemical energy storage, Adv. Mater. 24 (2012) 5166–5180.
[6] C. Yuan, L. Yang, L. Hou, L. Shen, X. Zhang, X.W. Lou, Growth of ultrathin mesoporous Co_3O_4 nanosheet arrays on Ni foam for high-performance electrochemical capacitors, Energy Environ. Sci. 5 (2012) 7883–7887.
[7] S. Surnev, A. Fortunelli, F.P. Netzer, Structure–property relationship and chemical aspects of oxide–metal hybrid nanostructures, Chem. Rev. 113 (2013) 4314–4372.
[8] W. Jung, K.L. Gu, Y. Choi, S.M. Haile, Robust nanostructures with exceptionally high electrochemical reaction activity for high temperature fuel cell electrodes, Energy Environ. Sci. 7 (2014) 1685–1692.
[9] I. Chang, S. Ji, J. Park, M.H. Lee, S.W. Cha, Ultrathin YSZ coating on Pt cathode for high thermal stability and enhanced oxygen reduction reaction activity, Adv. Energy Mater. 5 (2015) 1402251–1402257.
[10] Y. Choi, E.C. Brown, S.M. Haile, W. Jung, Electrochemically modified, robust solid oxide fuel cell anode for direct-hydrocarbon utilization, Nano Energy 23 (2016) 161–171.
[11] H.G. Seo, Y. Choi, B. Koo, A. Jang, W. Jung, Robust nano-architectured composite thin films for a low-temperature solid oxide fuel cell cathode, J. Mater. Chem. A 4 (2016) 9394–9402.
[12] D. Ding, X. Li, S.Y. Lai, K. Gerdes, M. Liu, Enhancing SOFC cathode performance by surface modification through infiltration, Energy Environ. Sci. 7 (2014) 552–575.
[13] W. Jung, J.O. Dereux, W.C. Chueh, Y. Hao, S.M. Haile, Energy Environ. Sci. 5 (2012) 8682–8689.
[14] M.A. Peña, J.L.G. Fierro, Chemical structures and performance of perovskite oxides, Chem. Rev. 101 (2001) 1981–2018.
[15] D.N. Mueller, M.L. Machala, H. Bluhm, W.C. Chueh, Redox activity of surface oxygen anions in oxygen-deficient perovskite oxides during electrochemical reactions, Nat. Commun. 6 (2015) 6097–6104.
[16] D. Chen, C. Chen, Z.M. Baiyee, Z. Shao, F. Ciucci, Nonstoichiometric oxides as low-cost and highly-efficient oxygen reduction/evolution catalysts for low-temperature electrochemical devices, Chem. Rev. 115 (2015) 9869–9921.
[17] E.N. Armstrong, K.L. Duncan, E.D. Wachsman, Effect of A and B-site cations on surface exchange coefficient for ABO_3 perovskite materials, Phys. Chem. Chem. Phys. 15 (2013) 2298–2308.
[18] K.C.-F. Leung, S. Xuan, X. Zhu, D. Wang, C.-P. Chak, S.-F. Lee, W.K.-W. Ho, B.C.-T. Chung, Gold and iron oxide hybrid nanocomposite materials, Chem. Soc. Rev. 41 (2012) 1911–1928.
[19] K. Sasaki, J. Tamura, H. Hosoda, T.N. Lan, K. Yasumoto, M. Dokiya, Pt–perovskite cermet cathode for reduced-temperature SOFCs, Solid State Ion. 148 (2002) 551–555.
[20] L. Dieterle, P. Bockstaller, D. Gerthsen, J. Hayd, E. Ivers-Tiffée, U. Guntow, Microstructure of nanoscaled $La_{0.6}Sr_{0.4}CoO_{3-\delta}$ cathodes for intermediate-temperature solid oxide fuel cells, Adv. Energy Mater. 1 (2011) 249–258.
[21] K.-I. Park, S. Xu, Y. Liu, G.-T. Hwang, S.-J.L. Kang, Z.L. Wang, K.J. Lee, Piezoelectric $BaTiO_3$ thin film nanogenerator on plastic substrates, Nano Lett. 10 (2010) 4939–4943.
[22] P. Plonczak, A. Bieberle-Hütter, M. Søgaard, T. Ryll, J. Martynczuk, P.V. Hendriksen, L.J. Gauckler, Tailoring of $La_xSr_{1-x}Co_yFe_{1-y}O_{3-\delta}$ nanostructure by pulsed laser deposition, Adv. Funct. Mater. 21 (2011) 2764–2775.
[23] A.R. Akbashev, G. Chen, J.E. Spanier, A facile route for producing single-crystalline epitaxial perovskite oxide thin films, Nano Lett. 14 (2014) 44–49.
[24] G.H.A. Therese, P.V. Kamath, Electrochemical synthesis of metal oxides and hydroxides, Chem. Mater. 12 (2000) 1195–1204.
[25] H.-C. Shin, J. Dong, M. Liu, Nanoporous structures prepared by an electrochemical deposition process, Adv. Mater. 15 (2003) 1610–1614.
[26] S.U. Rehman, R.-H. Song, T.-H. Lim, S.-J. Park, J.-E. Hong, J.-W. Lee, S.-B. Lee, High-performance nanofibrous $LaCoO_3$ perovskite cathode for solid oxide fuel cells fabricated via chemically assisted electrodeposition, J. Mater. Chem. A 6 (2018) 6987–6996.
[27] B.-K. Park, S.-B. Lee, T.-H. Lim, R.-H. Song, J.-W. Lee, High-performance solid oxide fuel cell with an electrochemically surface-tailored oxygen electrode, ChemSusChem, ⟨http://dx.doi.org/10.1002/cssc.201800962⟩.
[28] Y.B. Kim, C.-M. Hsu, S.T. Connor, T.M. Gür, Y. Cui, F.B. Prinz, Nanopore patterned Pt array electrodes for triple phase boundary study in low temperature SOFC, J. Electrochem. Soc. 157 (2010) B1269–B1274.
[29] T. Ryll, H. Galinski, L. Schlagenhauf, P. Elser, J.L.M. Rupp, A. Bieberle-Hutter, L.J. Gauckler, Microscopic and nanoscopic three-phase-boundaries of platinum thin-film electrodes on YSZ electrolyte, Adv. Funct. Mater. 21 (2011) 565–572.
[30] W. Jung, J.J. Kim, H.L. Tuller, Investigation of nanoporous platinum thin films fabricated by reactive sputtering: application as micro-SOFC electrode, J. Power Sources 275 (2015) 860–865.
[31] B.-K. Park, R.-H. Song, S.-B. Lee, T.-H. Lim, S.-J. Park, C.-O. Park, J.-W. Lee, Facile synthesis of Ca-doped $LaCoO_3$ perovskite *via* chemically assisted electrodeposition as a protective film on solid oxide fuel cell interconnects, J. Electrochem. Soc. 163 (2016) F1066–F1071.
[32] B.-K. Park, R.-H. Song, S.-B. Lee, T.-H. Lim, S.-J. Park, W. Jung, J.-W. Lee, Conformal bi-layered perovskite/spinel coating on a metallic wire network for solid oxide fuel cells *via* an electrodeposition-based route, J. Power Sources 348 (2017) 40–47.
[33] A. Takeshita, S. Miyoshi, S. Yamaguchi, T. Kudo, Y. Sato, High surface reactivity of La/Sr–Co perovskite based cathode with cation nonstoichiometry, Solid State Ion. 262 (2014) 378–381.
[34] S. Miyoshi, A. Takeshita, S. Okada, S. Yamaguchi, Rate-determining elementary step of oxygen reduction reaction at $(La,Sr)CoO_3$-based cathode surface, Solid State Ion. 285 (2016) 202–208.
[35] C. Ding, T. Hashida, High performance anode-supported solid oxide fuel cell based on thin-film electrolyte and nanostructured cathode, Energy Environ. Sci. 3 (2010) 1729–1731.
[36] E.D. Wachsman, K.T. Lee, Lowering the temperature of solid oxide fuel cells, Science 334 (2011) 935–939.
[37] Y. Chen, Y. Lin, Y. Zhang, S. Wang, D. Su, Z. Yang, M. Han, F. Chen, Low temperature solid oxide fuel cells with hierarchically porous cathode nano-network, Nano Energy 8 (2014) 25–33.
[38] H.G. Seo, Y. Choi, W. Jung, Exceptionally enhanced electrode activity of $(Pr,Ce)O_{2-\delta}$-based cathodes for thin-film solid oxide fuel cells, Adv. Energy Mater. 8 (2018) 1703647.
[39] S. Ji, W.H. Tanveer, W. Yu, S. Kang, G.Y. Cho, S.H. Kim, J. An, S.W. Cha, Surface engineering of nanoporous substrate for solid oxide fuel cells with atomic layer-deposited electrolyte, Beilstein J. Nanotechnol. 6 (2015) 1805–1810.

[40] J. An, Y.B. Kim, F.B. Prinz, Ultra-thin platinum catalytic electrodes fabricated by atomic layer deposition, Phys. Chem. Chem. Phys. 15 (2013) 7520–7525.
[41] T.P. Holme, R. Pornprasertsuk, F.B. Prinz, Interpretation of low temperature solid oxide fuel cell electrochemical impedance spectra, J. Electrochem. Soc. 157 (2010) B64–B70.
[42] C. Xia, Y. Lang, G. Meng, Recent advances to the development of low-temperature solid oxide fuel cells, Fuel Cells 4 (2004) 41–47.
[43] H. Huang, T. Holme, F.B. Prinz, Increased cathodic kinetics on platinum in IT-SOFCs by inserting highly ionic-conducting nanocrystalline materials, J. Fuel Cell Sci. Technol. 7 (2010) 041012.
[44] Y. Yan, S.C. Sandu, J. Conde, P. Muralt, Experimental study of single triple-phase-boundary and platinum-yttria stabilized zirconia composite as cathodes for micro-solid oxide fuel cells, J. Power Sources 206 (2012) 84–90.
[45] P.-C. Su, C.-C. Chao, J.H. Shim, R. Fasching, F.B. Prinz, Solid oxide fuel cell with corrugated thin film electrolyte, Nano Lett. 8 (2008) 2289–2292.
[46] A. Buyukaksoy, V. Petrovsky, F. Dogan, Solid oxide fuel cells with symmetrical Pt-YSZ electrodes prepared by YSZ infiltration, J. Electrochem. Soc. 160 (2013) F482–F486.
[47] K.-Y. Liu, Y.J. Yoon, S.H. Lee, P.-C. Su, Sputtered nanoporous PtNi thin film cathodes with improved thermal stability for low temperature solid oxide fuel cells, Electrochim. Acta 247 (2017) 558–563.